DOE/MC/30097 -- 5592
(DE97002239)

Task 6.6 - Sialon Coatings for Alkali-Resistant Silicon Nitride

Semi-Annual Report
July 1 - December 31, 1996

By
Jan W. Nowok

Work Performed Under Contract No.: DE-FC21-93MC30097

For
U.S. Department of Energy
Office of Fossil Energy
Morgantown Energy Technology Center
P.O. Box 880
Morgantown, West Virginia 26507-0880

By
Energy and Environmental Research Center
University of North Dakota
P. O. Box 9018
Grand Forks, North Dakota 58202-9018

Disclaimer

TABLE OF CONTENTS

LIST OF FIGURES

LIST OF TABLES

DISCLAIMER

ACKNOWLEDGMENT

This report was prepared with the support of the U.S. Department of Energy (DOE), Morgantown Energy Technology Center, Cooperative Agreement No. DE-FC21-93MC30097. However, any opinions, findings, conclusions, or recommendations expressed herein are those of the author(s) and do not necessarily reflect the views of the DOE.

EERC DISCLAIMER

SUBTASK 6.6 - SIALON COATINGS FOR ALKALI-RESISTANT SILICON NITRIDE

1.0 INTRODUCTION

The efficiency of a gas turbine can be improved by increasing operating temperature. Construction materials should meet both high-strength requirements and hot-alkali corrosion resistance. Structural ceramics based on silicon nitride are promising candidates for high-temperature engineering applications because of their high strength and good resistance to corrosion. Their performance varies significantly with the mechanical properties of boundary phases which, in turn, depend on their chemical composition, thickness of the amorphous phase, and the deformation process. To make silicon nitride ceramics tough, SiAlON ceramics were developed with controlled crystallization of the amorphous grain boundary phase. Crystallization of the grain boundary glass improves the high-temperature mechanical properties of silicon nitride ceramics.

Two SiAlON phases, α- and β-, are isostructural with α- and β-silicon nitride[1] and offer a unique combination of mechanical properties for silicon nitride-based ceramics that enhance their performance in gas turbine applications.[2,3] There is, however, a corrosion problem of Si_3N_4 caused by alkalies, especially under combustion conditions. Typical corrosion in gas turbine material has been called Na_2SO_4 attack and results from the formation of a sodium-silicate liquid phase at temperatures above approximately 800°C, the eutectic temperature in the sodium-silica system. Usually, Na_2SO_4 is formed by the reaction of NaCl (both solid particles and vapor) with SO_2 when the SO_2 content in flue gas is above the equilibrium of sulfur dioxide partial pressure over Na_2SO_4. SiAlON-Y ceramics offer more resistance in terms of hardness, elastic moduli, and corrosion.[4] Oxidation of SiAlON ceramics is lower by one order of magnitude than that of hot-pressed Si_3N_4 and in the same order of that of reaction-sintered Si_3N_4. It is recognized that the oxidation rate decreases with increased of Al content.[5] Also, the addition of Y_2O_3, Nd_2O_3, La_2O_3, Sm_2O_3, and CeO_2 as sintering aids to SiAlON greatly reduces both its oxidation rate and its densification temperature by forming a eutectic liquid phase.[6-8] It seems generally accepted that the oxidation kinetics of both SiAlON and Si_3N_4 ceramics are strongly related to the rapid diffusion of oxygen formed during corrosion of ceramics through the silicate melt, and this depends on both the volume and the chemical composition of the intergranular phase(s).[9-13] It has also been suggested that SiAlON ceramic may be used as an oxidation barrier on TiAl6V4 alloy.[6, 14,15]

Thus, the knowledge of silicon oxynitride ceramics corrosion behavior in Na_2SO_4 becomes important for engineers in designing appropriate parts for turbines working at high temperatures. So far there has been no report concerning alkalies attack of SiAlON ceramics in the presence of SO_2 and chlorine in flue gas. The goal of this project is to investigate alkali corrosion of SiAlON-Y structural ceramics under combustion conditions in the presence of sodium-derived components.

2.0 DESIGN OF EXPERIMENTAL PROCEDURE

Generally, the corrosion process of any material as well as structural ceramic is controlled by the nature of the products produced by the chemical reactions between active components in the gas (liquid) phase and the ceramic and by mass transport phenomena, both inward to and out from the

ceramic. However, the products formed in the corrosion process depend on the concentration of active components in the gas (liquid) phase, temperature, reaction time, and atmosphere (oxidizing and/or reducing). Atmosphere may have a significant effect on the mass transport phenomena of active components because of preoxidization of the ceramic's surface and/or generation of nonstoichiometry under reducing conditions. Also, the porosity of the solid; the wetability of the solid phase by the formed liquid phase; the viscosity of the liquid phase; any gradients such as concentration and temperature; geometry of the samples; and stresses generated in the thin film at the interface resulting from the solid–gas (liquid) chemical reaction can influence the corrosion process.

The first step in the corrosion tests was to determine the composition of the gas generated in combustion and/or gasification environments. Thermochemical equilibria can be used to derive information on alkali composition in the vapor phase over any solid phase such as an ash. We used the FACT (Facility for the Analysis of Chemical Thermodynamics) code developed by C.W. Bale, A.D. Pelton, and W.T. Thomson from Ecole Polytechnique de Montréal, Canada.

Using the FACT code, we calculated the quantities of stable alkali phases in vapor over an ash (the composition is listed in Table 1) and pure components in the presence of SO_2 (1000 ppm), Cl_2 (100 ppm), and H_2O (15 vol% of total gas) under combustion conditions. An example of variation in quantities of alkalies in a vapor phase with temperature under combustion conditions is presented in Figure 1. The six stable alkali phases showing the highest mole percent are KCl, NaCl, KOH, NaOH, K_2SO_4, and Na_2SO_4. These phases by no means represent all possible active components in the corrosion process of Si_3N_4 and SiAlON structural ceramics. Usually, sulfates rather than chlorides and hydroxides are taken into account as active corrosion components.

TABLE 1

Ash Composition (wt% expressed as equivalent oxide)								
SiO_2	Al_2O_3	Fe_2O_3	TiO_2	P_2O_5	CaO	MgO	Na_2O	K_2O
44.6	19.4	8.9	0.7	0.3	13.5	10.1	0.6	1.8

3.0 EXPERIMENTAL PROCEDURE

Two SiAlON ceramic bars of varied yttrium content were prepared with pressureless sintering powders of silicon nitride, aluminum oxide, aluminum nitride, and yttrium oxide at 1650°C for 5 hr in a nitrogen atmosphere with 2 vol% of hydrogen. The composition of SiAlON-Y was restricted mainly to the composition of β-SiAlON, of which the thermal expansion coefficient (2×10^{-6}) deg^{-1} is close to that of β-Si_3N_4 ceramic (3×10^{-6} deg^{-1}).[16] The composition of the starting powders expressed in a mole fraction is as follows: (A) $Si_3N_4 = 0.23$, AlN = 0.48, $Al_2O_3 = 0.26$, $Y_2O_3 = 0.03$ and (B) $Si_3N_4 = 0.306$, AlN = 0.306, $Al_2O_3 = 0.306$, $Y_2O_3 = 0.08$. The equimolar amounts of Si_3N_4, AlN, and Al_2O_3 prepared prior to high-temperature sintering stabilize the important single-phase β-SiAlON.[7] The starting powders were carefully weighed and stirred in water-free propanol using a blender for 5 hr. The mixture was then vacuumed-dried at 150°C before sintering. The density of the sintered samples was determined by pycnometric technique.

Crystalline phases formed in the sintered SiAlON-Y ceramics were identified by x-ray diffraction (XRD) and scanning electron microscopy (SEM).

Prior to corrosion testing, the SiAlON-Y ceramic bars were cut to 30- × 30- × 5-mm disks using a diamond saw and were polished, cleaned in ethanol, and dried in air. Corrosion tests were performed at 1100°, 1200°, and 1300°C for various time periods in both the sodium sulfate and sodium chloride vapors. The sodium sulfate and chloride were vaporized at 800°C in separate furnace and transported into the reaction section by a mixture of SO_2 (100 ppm) and air. The partial pressures of Na_2SO_4 and NaCl over pure substances at 800°C correspond to those above coal, as indicated on Figure 1. Disks of SiAlON-Y were weighed before and after corrosion tests. Morphology tests and measurements of the thickness of the corrosion layers were performed on cross-sectioned, polished samples using SEM sodium line scans.

Also, corrosion tests of SiAlON-Y samples were performed in liquid Na_2SO_4 and in a coal ash slag (composition is listed in Table 2), at 1200°C as a function of time. These tests have allowed comparison between the corrosion rate of SiAlON-Y ceramics and similar corrosion tests cited in the literature for other structural ceramics such as Si_3N_4.[17,18] The corrosion kinetics of SiAlON-Y ceramics in liquid Na_2SO_4 were determined from the thickness of the corrosion layers as measured by SEM.

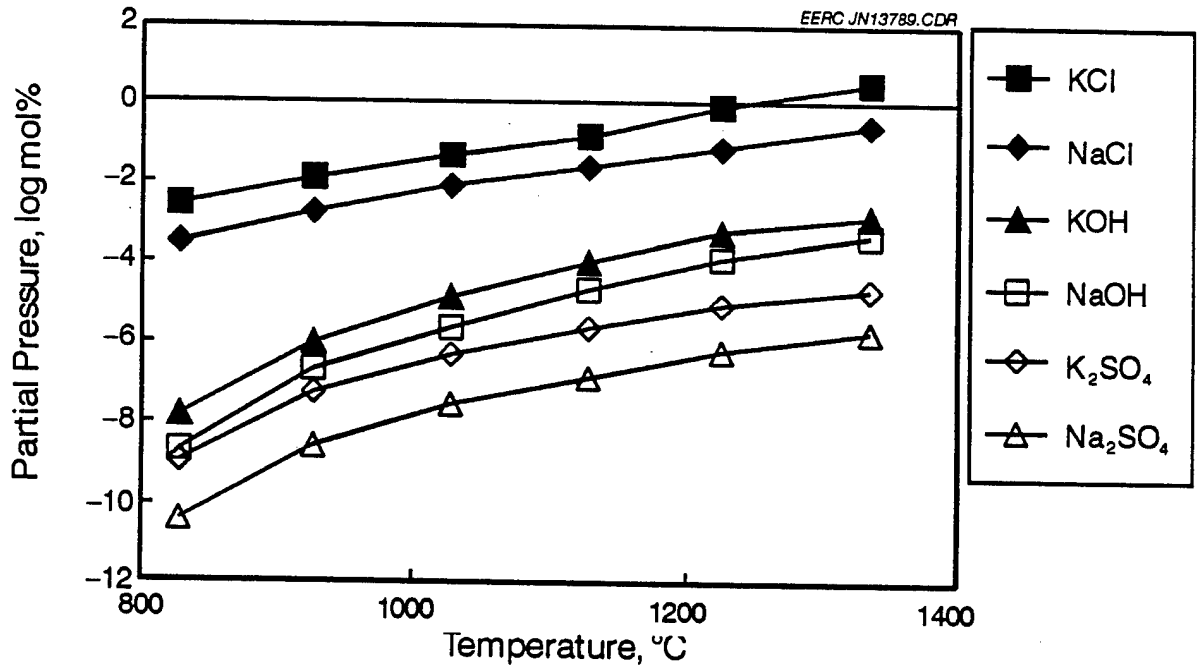

Figure 1. Distribution of alkali chlorides, hydroxides, and sulfates in a vapor phase over ash as a function of temperature in a combustion environment.

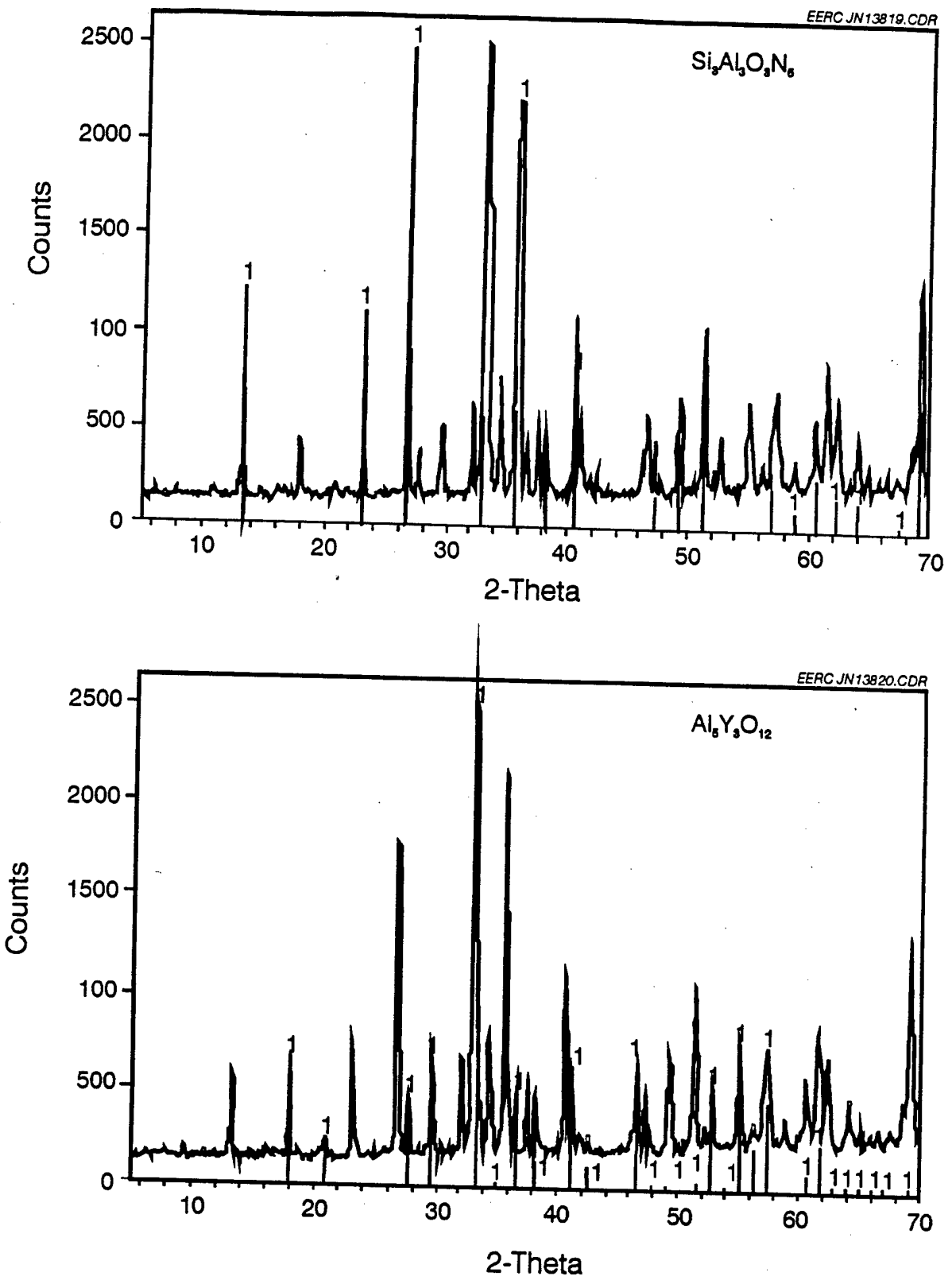

Figure 2. X-ray diffraction patterns of SiAlON-Y ceramic with diffraction lines of $Si_3Al_3O_3N_5$ and $Al_5Y_3O_{12}$ phases indicated.

TABLE 2

Ash Slag Composition (wt% expressed as equivalent oxide)

SiO_2	Al_2O_3	Fe_2O_3	TiO_2	P_2O_5	CaO	MgO	Na_2O	K_2O
28.1	14.4	10.1	2.7	0.4	27.3	5.7	10.1	1.2

4.0 EXPERIMENTAL RESULTS AND DISCUSSION

4.1 Structure and Morphology of SiAlON-Y Ceramics

Figure 2 shows x-ray diffraction patterns of SiAlON-Y ceramics after sintering at 1650°C for 5 hr. Two major phases are identified: silicon aluminum oxide nitride, $Si_3Al_3O_3N_5$, which corresponds to β-SiAlON[8] ($Si_{6-x}Al_x\ O_x\ N_{8-x}$, where x = 3) and aluminum yttrium oxide ($Al_5Y_3O_{12}$), respectively. The latter phase pertains to crystalline precipitates formed during the sintering process (Figure 3). The densities of sintered SiAlON-Y ceramics are for Ceramic A 2.828 (± 0.004)·10^3 kg/m^3 and for Ceramic B 2.996 (± 0.008)·10^3 kg/m^3, which values are lower than the theoretical density of the $Si_3Al_3O_3N_5$ phase, 3.095·10^3 kg/m^3, likely because of the presence of fine pores.[19] Fine porosity samples were lower than 3% as estimated using automated image analysis of backscattered electron images by SEM.

Figure 3 illustrates the microstructure of the β-SiAlON-Y and β-Si_3N_4 interface and distribution of aluminum and silicate elements along the scan line as indicated on the microstructure. Generally, the interface is enriched in aluminum yttrium oxide precipitates. This indicates a high rate of diffusion of yttrium ions along grain boundaries into the interface during the sintering process. The sintering of SiAlON-Y starting powders with composition (B) and β-Si_3N_4 bars, purchased from Norton Company, was performed at 1650°C for 3 hr in a nitrogen atmosphere with 2 vol% of H_2. The results suggest that β-SiAlON-Y ceramics create a good joint with β-Si_3N_4 bars without generating any cracks as the samples are cooled to room temperature. This is highly significant information with regard to both joining silicon nitride bars to larger ones and the formation of ceramic coatings.

4.2 Corrosion of β-SiAlON-Y Ceramics in Sodium Sulfate and Chloride Vapor

Figures 4 and 5 illustrate corrosion mass change for two β-SiAlON-Y ceramics at 1100°, 1200°, and 1300°C for up to 100 hr in Na_2SO_4 NaCl vapor (about 10^{-6} torr). Generally, the corrosion process for these ceramics increases with temperature and is lower for SiAlON, which has higher yttrium content. The corrosion process decreases at 1300°C after 20 hr of sample exposure to sodium sulfate and sodium chloride vapor, the result of an increase in crystalline precipitate content for both $Y_{14}Si_3O_{12}$ and $Y_{14}Al_3O_{12}$ phases in the surface layers as identified from XRD patterns and by energy-dispersive x-ray analysis coupled with SEM (Figure 6). The diffusion of yttrium ions into the surface causes the formation of yttrium-rich oxide barriers to sodium diffusion into the bulk of the ceramic, leaving a depletion zone of yttrium precipitates. The lower-sodium aluminate, $NaAlO_2$, and silica are also evident in the surface layers. No sodium silicate phase has been noted in analyzed specimens.

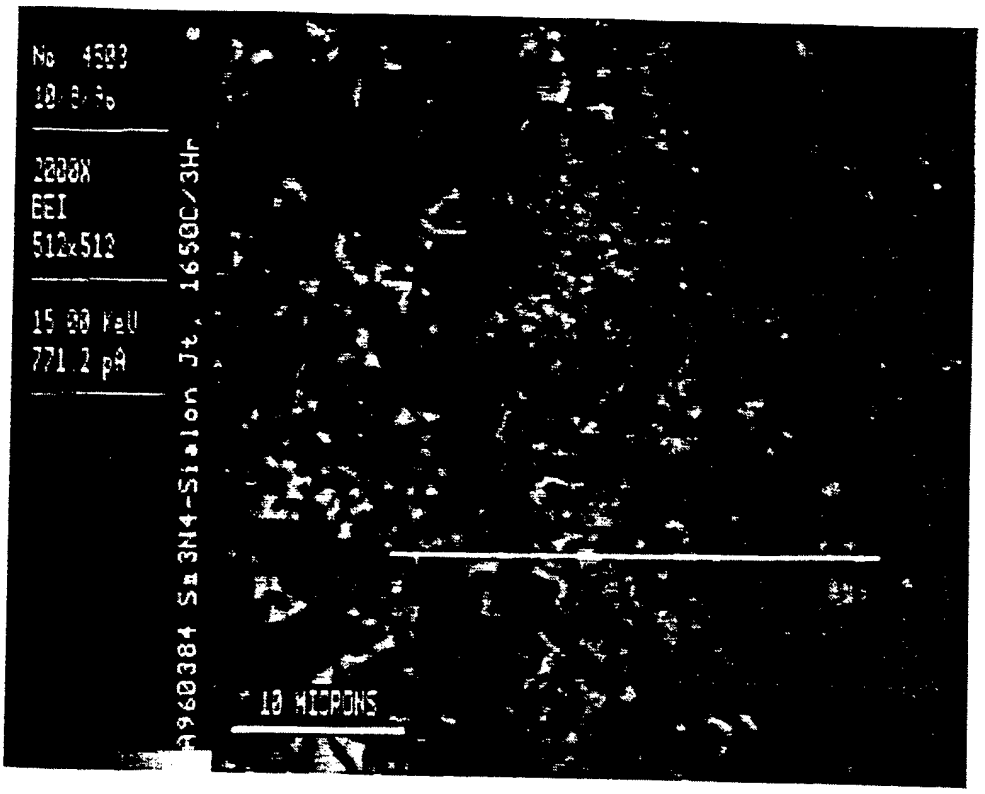

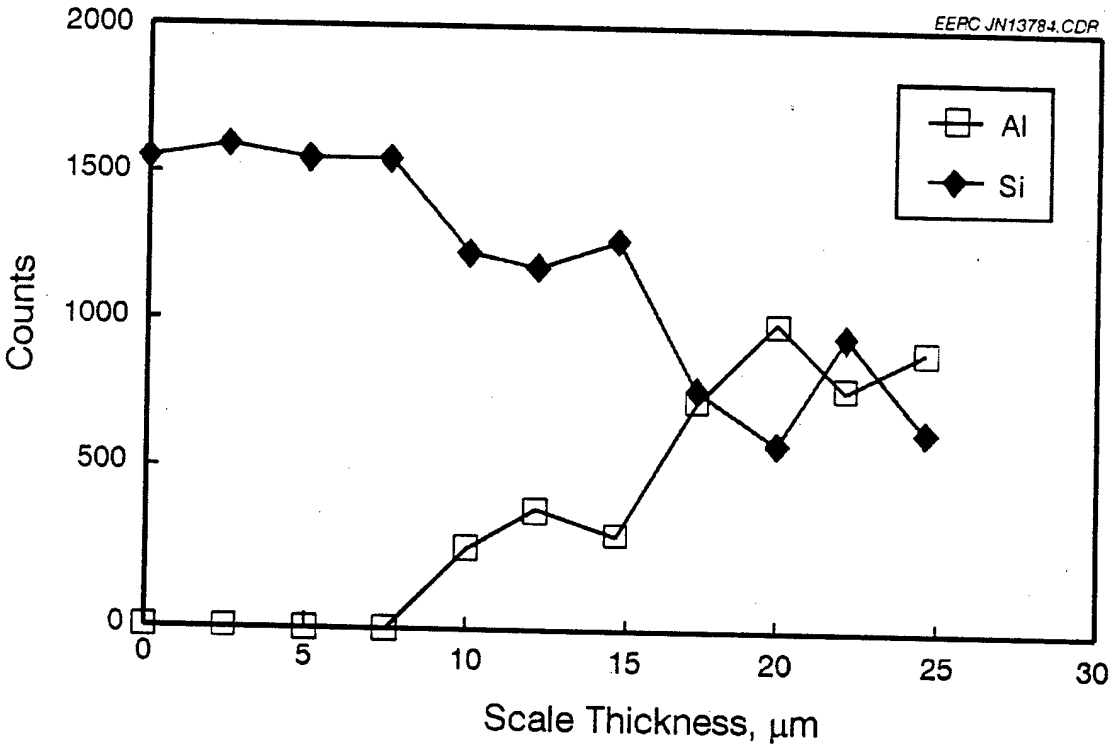

Figure 3. Microstructure of the β-Si_3N_4 and β-SiAlON-Y interface and distribution of Al and Si elements at the interface.

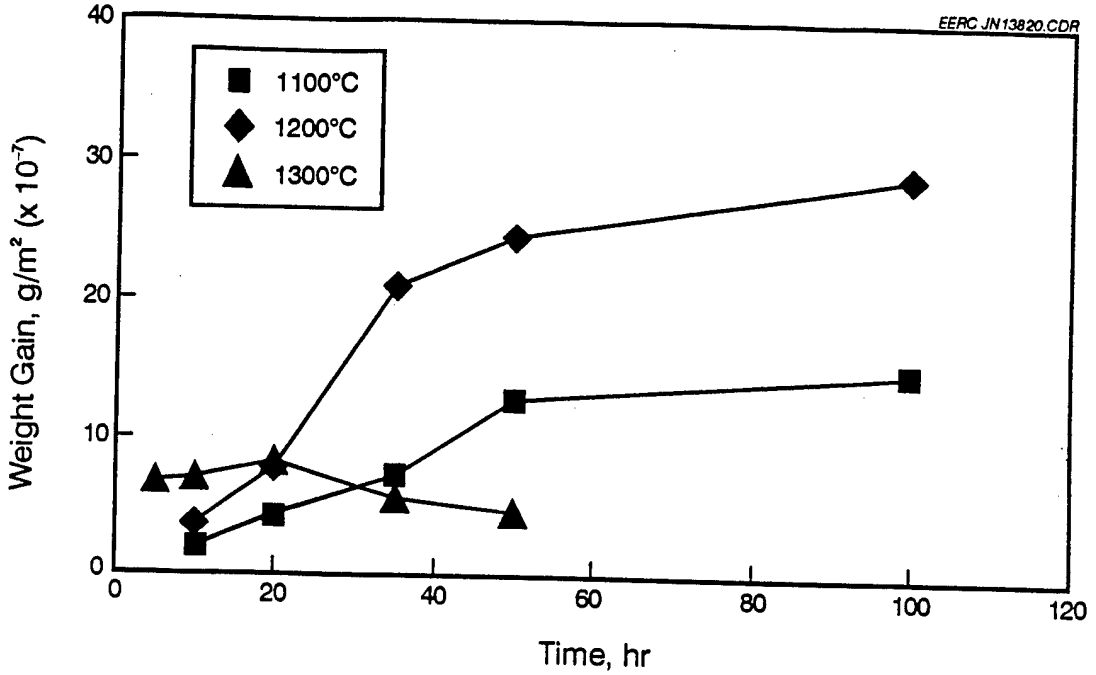

Figure 4. Corrosion mass change in β-SiAlON-Y ceramic (Composition A) as a function of time at various temperatures.

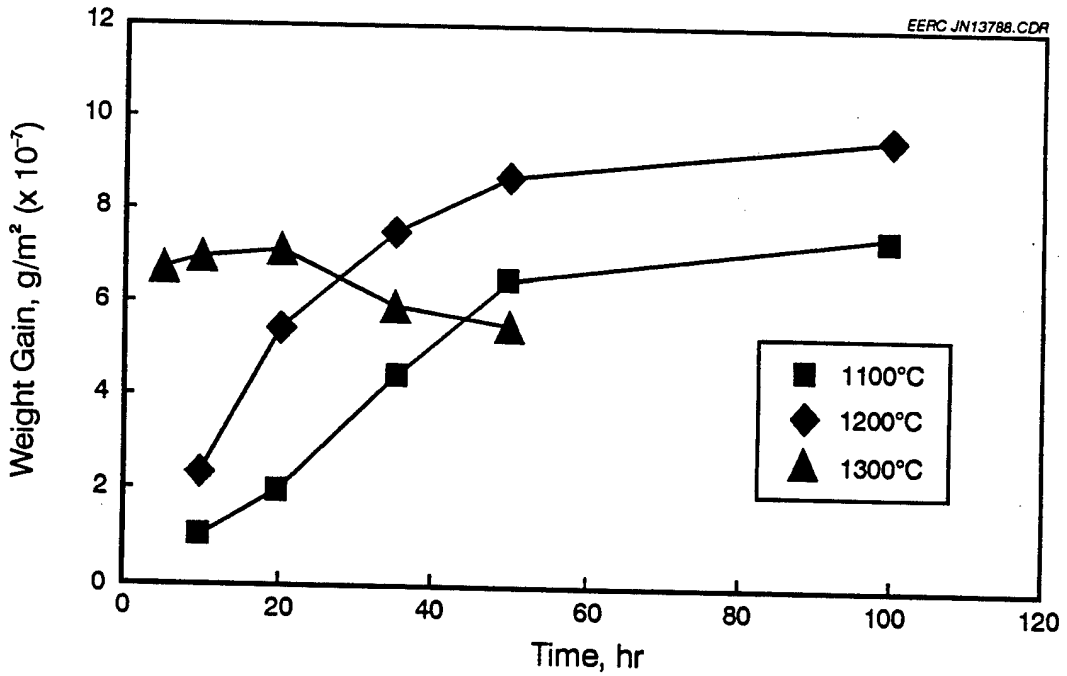

Figure 5. Corrosion mass change in β-SiAlON-Y ceramic (Composition B) as a function of time at various temperatures.

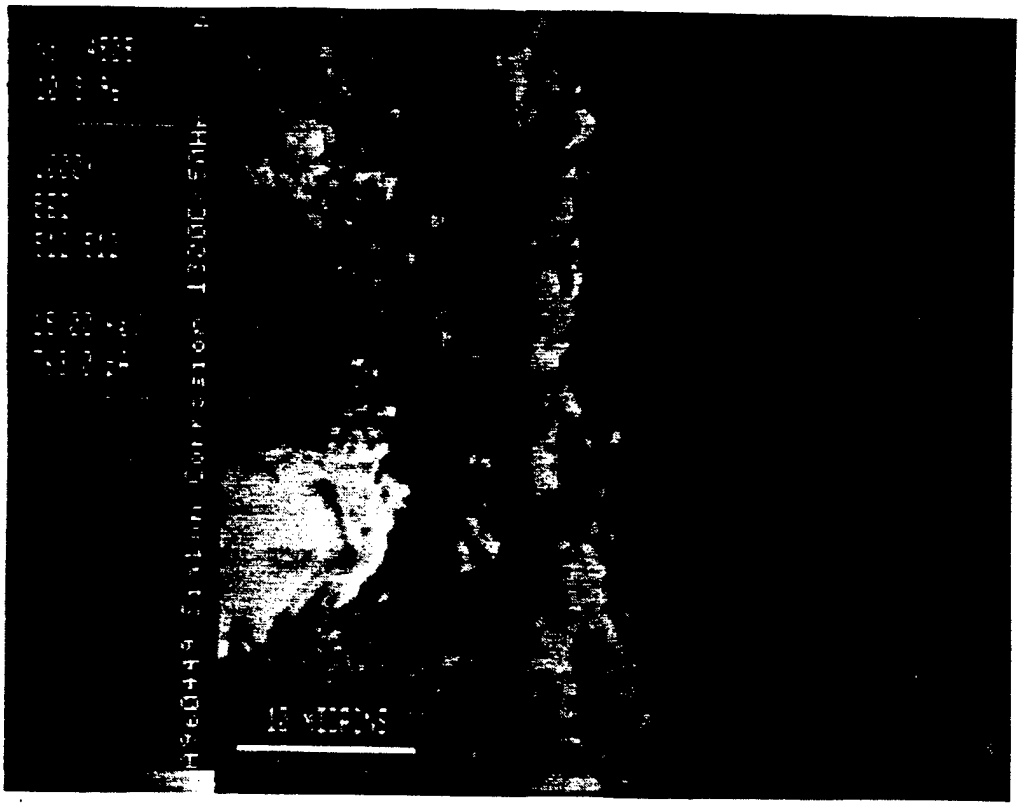

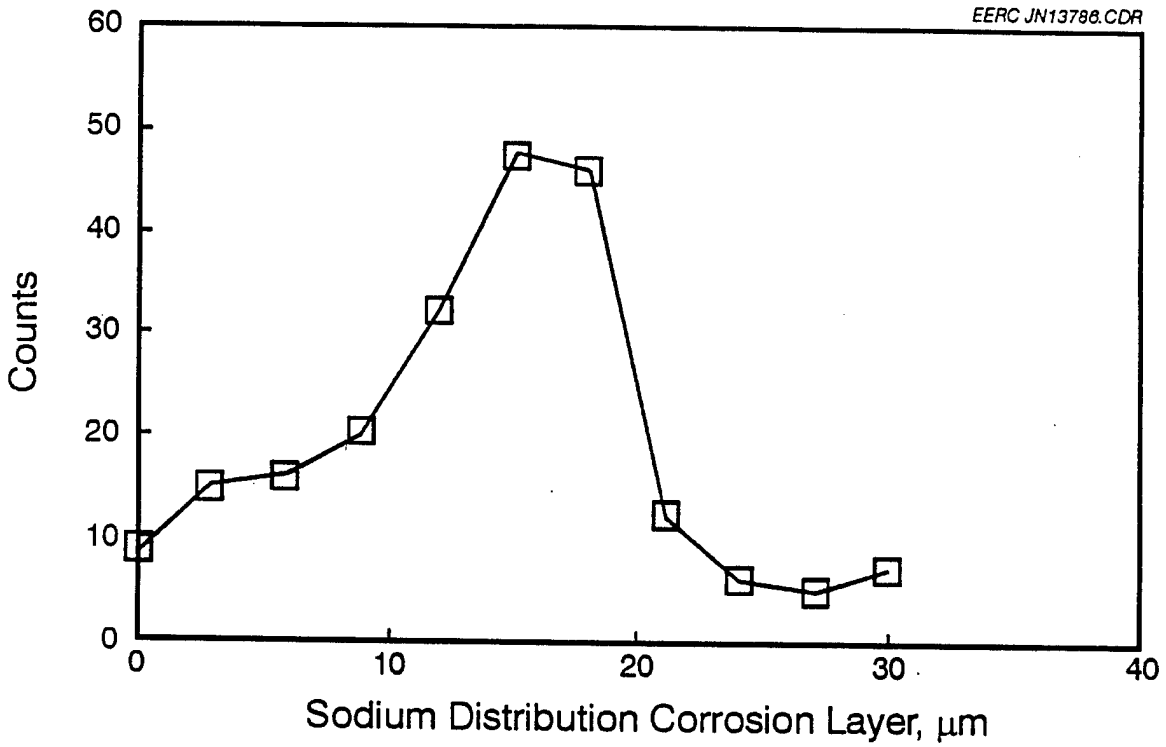

Figure 6. Microstructure of β-SiAlON-Y ceramic (Composition A) and sodium distribution in surface layers after corrosion in sodium vapor at 1300°C for 50 hr.

Figure 7 shows secondary and backscattered images of the surface of selected β-SiALON-Y ceramic with drops of sodium-rich silicate (a) and yttrium-rich phases beneath the drops (b), respectively formed during the first hours of ceramic corrosion at 1300°C. The corroded surface contains bubbles, most likely of nitrogen oxide(s), and this indicates that silicate melt formed during the corrosion process had a higher viscosity.

The corrosion mechanism of β-SiAlON-Y might be explained by the following chemical reactions thought to occur between β-SiAlON ceramics and sodium vapor:

$$2Si_3Al_3O_3N_5 + 3Na_2O + 17.5O_2 = 6NaAlO_2 + 6SiO_2 + 10NO_2 \quad [1]$$

The above reaction can be also written in a more general way:

$$4SiAlON + 2Na_2O + 9O_2 = 4NaAlO_2 + 4SiO_2 + 4NO_2 \quad [2]$$

Measurements of corrosion thickness on β-SiAlON-Y ceramics using sodium line scanning confirm the corrosion reduction at 1300°C above 20 hr (Figure 8) as previously presented in Figures 4 and 5. The improved sodium corrosion resistance of β-SiAlON-Y ceramics is caused by the yttrium-rich phases formed during the corrosion process rather than silica, and these phases are directly related to the yttrium content of the ceramics. Higher yttrium content corresponds to higher corrosion resistance of β-SiAlON ceramics to alkalies. The depletion zone of yttrium and the formation of corrosion-protective layers seem to be caused by a dissolution–reprecipitation mechanism in yttrium-rich phases. At the present time, we do not know whether sodium dissolved in the surface layers of β-SiAlON-Y ceramics promotes the dissolution–reprecipitation mechanism of yttrium-rich oxides.

Generally, the corrosion-protective layers formed on metals and alloys are controlled by the lattice diffusion of atoms or ions of the reactants or the transport of electrons through the scales. This type of transport process is parabolic with time and takes place because of the presence of point defects. Our preliminary calculations for β-SiAlON-Y ceramic using the Wagner theory[20]:

$$x^2 = 2k_p' + C \quad [3]$$

and/or

$$(\Delta m/S)^2 = 2k_p' + C \quad [4]$$

where x denotes the thickness of a corrosion layer, $\Delta m/S$ represents weight gain per unit of surface, k_p' is the parabolic rate constant, and C is the integration constant, exclude a parabolic corrosion mechanism. This conclusion is consistent with that previously derived by Persson et al. in the discussion of the oxidation mechanism of β-SiAlON-Y.[8]

4.3 Corrosion of β-SiAlON-Y Ceramics in Sodium Sulfate and Chloride Melt

Corrosion of β-SiAlON-Y ceramic in a molten Na_2SO_4 and NaCl mixture at 1200°C does not significantly vary from that in a vapor phase. Figure 9 illustrates variation in corrosion thickness with time compared to that for β-SiAlON-Y ceramics exposed to the vapor phase. Generally, the corrosion rate in β-SiAlON-Y ceramics observed in a melt is higher. Also,

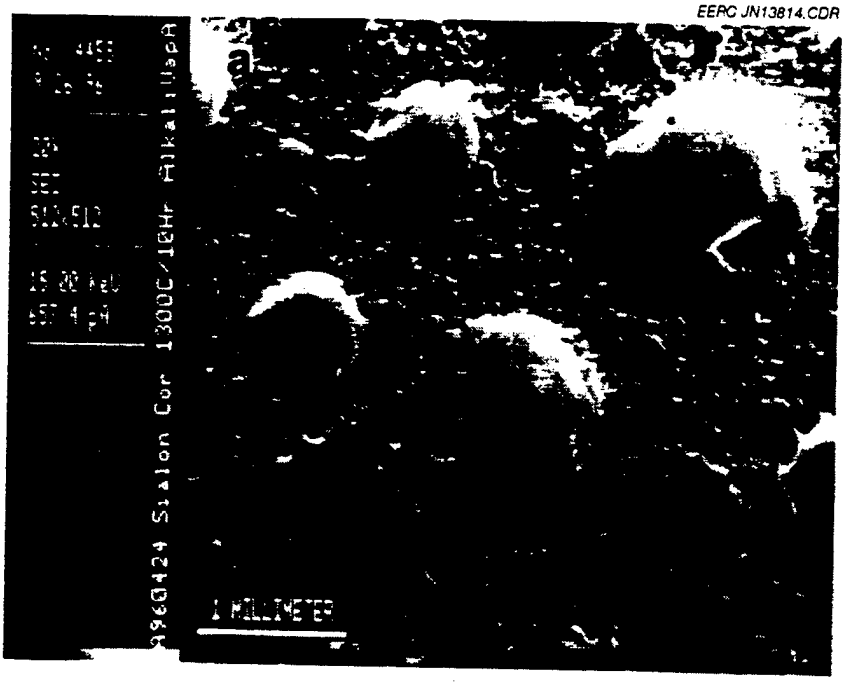

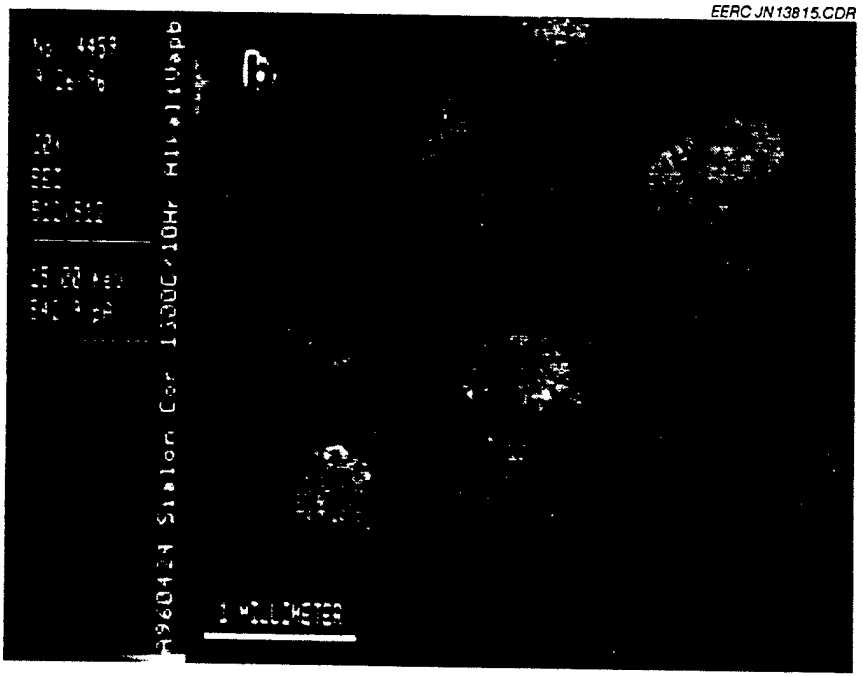

Figure 7. Secondary (a) and backscattered (b) images of SiAlON-Y surfaces (Composition B) after corrosion in Na_2SO_4 vapor for 10 hr.

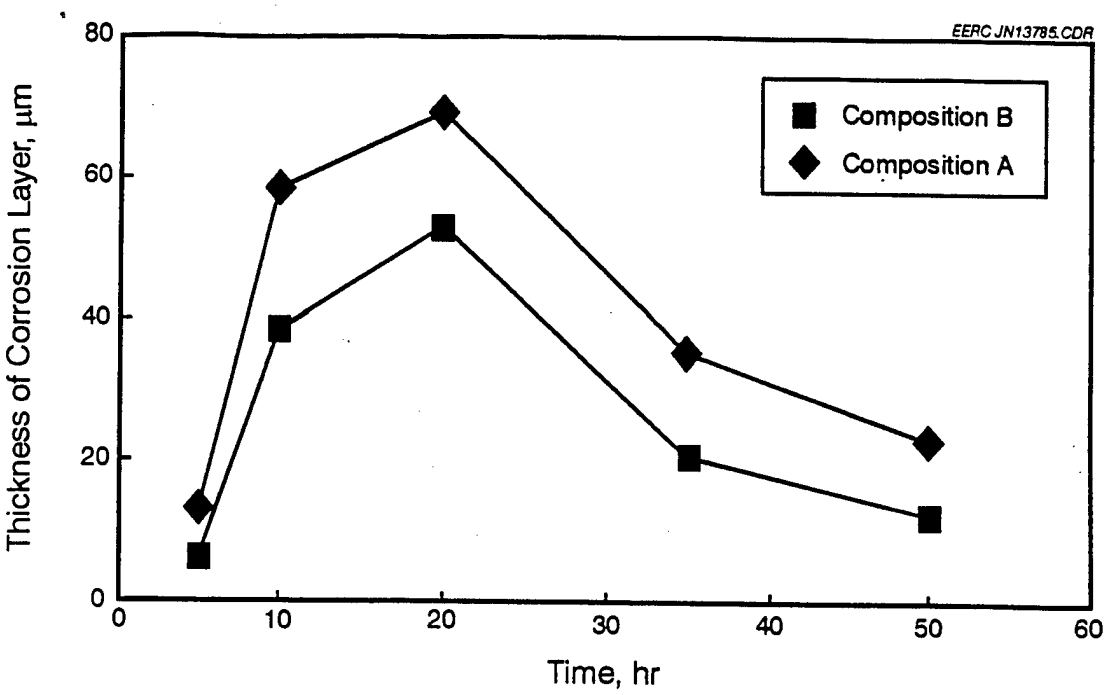

Figure 8. Change in corrosion thickness in β-SiAlON-Y at 1300°C.

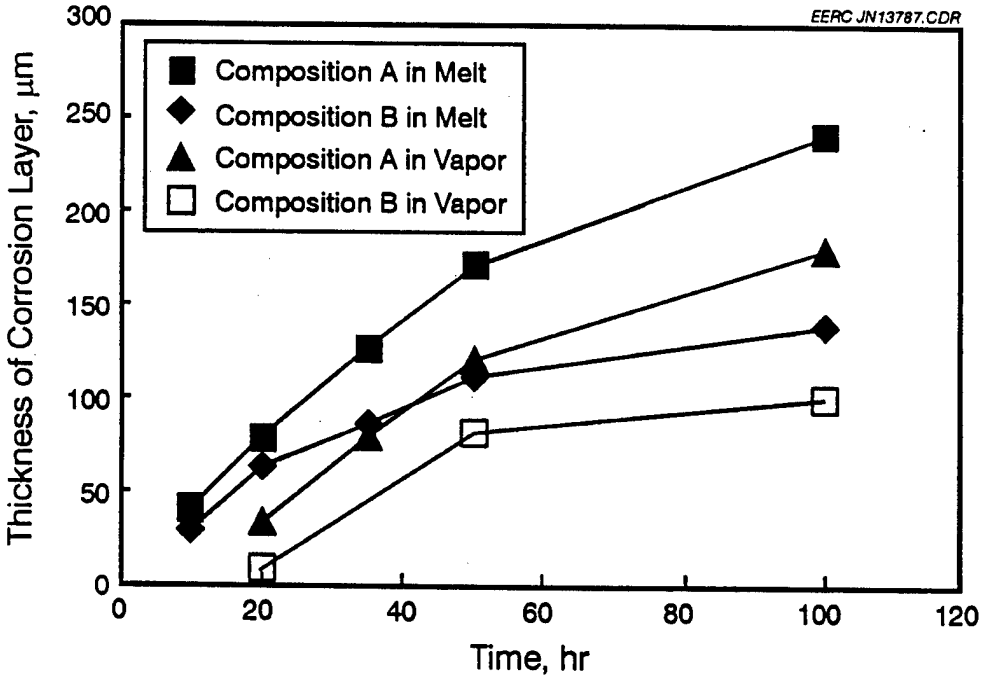

Figure 9. Change in corrosion thickness in β-SiAlON-Y at 1200°C after corrosion in Na_2SO_4 melt and Na_2SO_4 + NaCl vapor.

higher porosity is observed in the corrosion layers as a result of more nitrogen oxide gas being given off as one of the corrosion products. In samples exposed for a longer time to liquid salt, the corrosion layers partially delaminate and spall during cooling to room temperature (Figure 10). Na_2O–Al_2O_3–SiO_2 silicates are formed on the surface as a corrosion product. Thus, the deleterious reaction of sodium with SiAlON-Y in the presence of sulfur and chlorine may become possible through the formation of cracks as a result of localized stress gradients, likely generated by both silica and silicate content. This corrosion mechanism was already recognized in both silicon carbide and nitride ceramics.[17] Usually, the corrosion of silicon nitride by molten salts occurs in three stages: 1) formation of sodium silicate, lasting only minutes, 2) inward diffusion of molecular oxygen to the silicon nitride surface layers, forming silica, and 3) oxygen diffusion in silica.

4.4 Corrosion of β-SiAlON-Y Ceramics in Ash Slag

The corrosion mechanism of β-SiAlON-Y ceramic in ash slag does not vary from that discussed above at 1200°C and is also related to the diffusion of both sodium and potassium into the samples bulk. Figure 11 illustrates the β-SiAlON-Y/slag interface, and Table 3 lists atom percent of major elements near the interface. Generally, yttrium content increases at the interface as a result of the precipitation of yttrium-rich phases, which creates barriers to sodium and potassium atom diffusion into the bulk of the β-SiAlON ceramic and simultaneously increases its resistance to alkali corrosion. Practically, the β-SiAlON-Y ceramic is not significantly affected by ash slag.

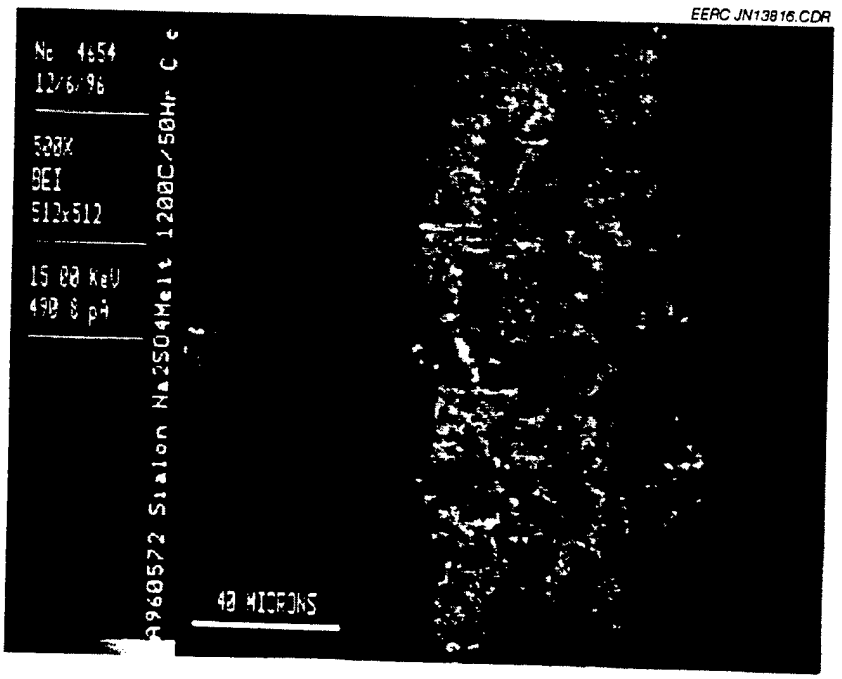

Figure 10. Microstructure of β-SiAlON-Y specimen after corrosion in molten Na_2SO_4-NaCl melt at 1200°C for 50 hr.

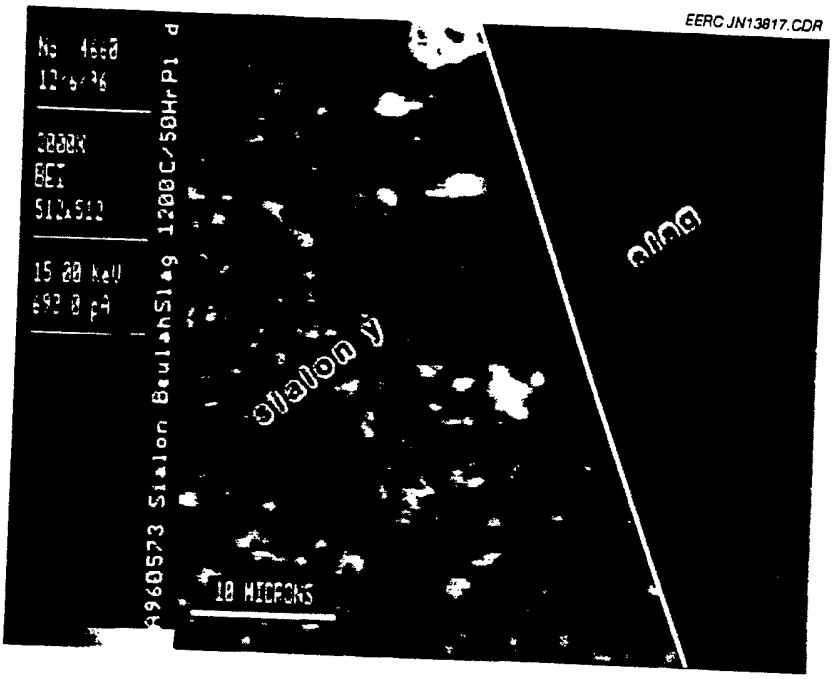

Figure 11. β-SiAlON-Y/slag interface formed during ceramic corrosion in ash slag at 1200°C for 100 hr.

TABLE 3

Atomic Percent of Major Elements Near the β-SiALON-Y–Slag (B) Interface*

Element	Bulk of SiAlON-Y	Bulk SiAlON-Y/ SiAlON Interface	SiAlON/ Slag Interface	Bulk Slag
Na	0.0	0.3	0.3	3.6
K	0.0	0.2	0.1	0.4
Mg	0.0	0.0	0.5	2.7
Al	64.0	15.6	15.7	9.8
Si	22.5	49.5	14.9	14.9
Ca	0.0	0.0	6.5	7.4
Ti	0.0	0.0	0.0	0.3
Fe	0.0	0.2	0.6	2.2
Y	0.7	5.3	0.0	0.0

*Oxygen and nitrogen are not included. Corrosion conditions: 1200°C and 100 hr.

5.0 CONCLUSIONS

It has been demonstrated that yttrium-rich phases precipitated at the surface of β-SiAlON-Y ceramics increase their corrosion resistance to an alkali environment at high temperatures. The corrosion behavior is nonparabolic, likely, as a result of the dissolution–reprecipitation process of

the yttrium-rich phases and/or the formation of high-viscosity silicate melt within the corrosion layers, in which the diffusion of corrosion-active components cannot be described by the parabolic rate law.

6.0 REFERENCES

1. Iseki, T. ; Hase, T. In *Fine Ceramics;* Saito, S., Ed.; Elsevier Applied Science Publishers, Ltd: Essex, England, 1985; p.188.

2. Lenoe, E.M.; Katz, R.N.; Burke, J.J. *Ceramics for High Performance Applications III. Reliability*, Plenum Press: New York, 1983.

3. Smyth, J.R. In *Ceramics and Glasses, Engineered Materials Handbook*, ASM International, 1991; Vol.4, p. 995.

4. Hampshire, S.; Drew, R.A.L.; Jack, K.H. *Phys. Chem. Glasses* **1985**, *26*, 182.

5. Knotek, Otto; Löffler, F.; Beele, W. *Mat. Res. Soc. Symp. Proc.* **1993** *287*, 539.

6. Ekström, T.; Nygren, M., *J. Am. Ceram. Soc.* **1992**, *75*, 259.

7. Mieskowski, D.M.; Sanders, W.A. *J. Am. Ceram. Soc.* **1985** *68*, C-160.

8. Persson, J.; Ekström, T.; Per-Olov Kall; Nygren, M. *J. Europ. Ceram. Soc.* **1993**, *11*, 363.

9. Singhal, S.C.; Lange, F.F. *J. Am. Ceram. Soc.* **1977**, *60*, 190.

10. Schlichting, J.; Gauckler, L. *J. Powder Metall. Int.* **1977**, *9*, 36.

11. Lewis, M.H.; Bernard, P. *J. Mater, Sci.* **1980**, *15*, 443.

12. Babini, G.N.; Bellosi, A.; Vincenzini, P.A. *J. Mater. Sci.* **1984**, *19*, 1029.

13. Patel, J.K.; Thomson, D.P. *Brit. Ceram. Trans J.* **1988**, *87*, 70.

14. Ekström, T. *Mat. Res. Soc. Symp.* **1993**, *287*, 121.

15. Schlichting, J. *Nitrogen Ceramics;* Riley, F.L., Ed.; Noordhoff: Leyde, 1977; p. 627.

16. Tien, T. *Mater. Sci. Eng.* **1993**, *51A*, 287.

17. Munro, R.G.; Dapkunas, S.J. *J. Res. Natl. Inst. Stand. Technol.* **1993**, *98*, 607.

18. Shinata, Y.; Hara, M.; Nakagawa, T.; Shimizu, Ch. In *High Temperature Corrosion of Advanced Materials and Protective Coatings*, Saito, Y.; Önay, B; Maruyama, T., Eds.; Elsevier Science Publishers: Amsterdam, 1992; p. 365.

19. ASTM Card No. 36-1333. Visser, J., "Technisch Physische Dienst," Delft, Netherlands, ICDD Grant, 1984.

20. Kofstad, P. In *High Temperature Corrosion of Advanced Materials and Protective Coatings*; Saito, Y.; Omay, B.; Marimba, T., Eds.; Elsevier: Amsterdam, 1992; p. 3.

J-BAY4T6Q4

FORM EIA-459E
(10/88)

U.S. DEPARTMENT OF ENERGY
FEDERAL ASSISTANCE MANAGEMENT SUMMARY REPORT

FORM APPROVED
OMB NO. 1900 0127

1. Program/Project Identification No.	2. Program/Project Title	3. Reporting Period
DE-FC21-93MC30097	TASK 6.0 HIGH-TEMPERATURE MATERIALS	10-1-96 through 12-31-96

4. Name and Address: Energy & Environmental Research Center, University of North Dakota, PO Box 9018, Grand Forks, ND 58202-9018 (701) 777-5000

5. Program Start Date: 01-12-93

6. Completion Date: 12-31-97

7. FY: 96/97

8. Months or Quarters: Quarters

9. Cost Status: a. Dollars Expressed In Thousands

b. Dollar Scale

1st			2nd			3rd			4th		
JAN	FEB	MAR	APR	MAY	JUN	JUL	AUG	SEP	OCT	NOV	DEC

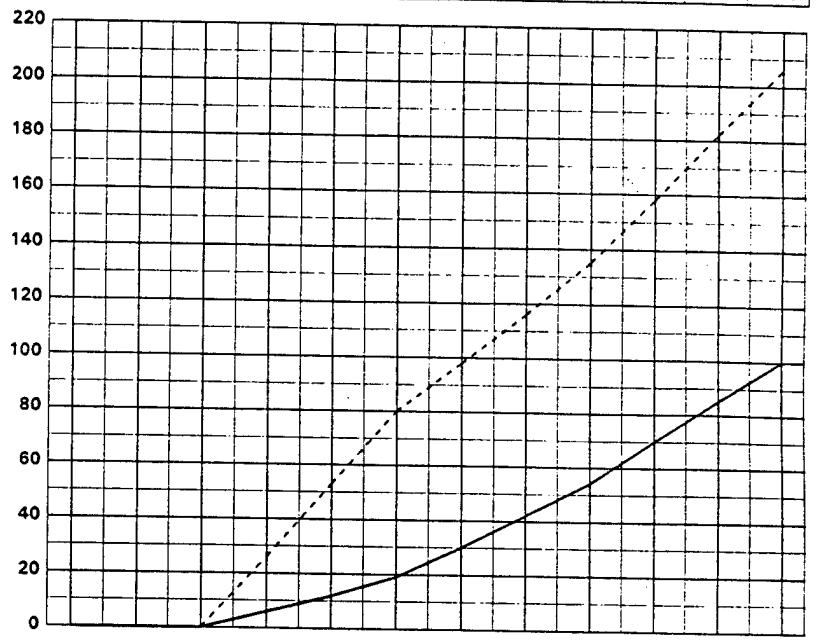

10. Cost Chart

Fund Source		Quarter 1st	2nd	3rd	4th	Cum. to Date	Tot. Plan
DOE	P	0	80	55	71	206	206
	A	0	19	35	46	100	
	P						
	A						
	P						
	A						
	P						
	A						
Total P		0	80	55	71	206	206
Total A		0	19	35	46	100	
Variance		0	61	20	25	106	

P = Planned A = Actual

Total Planned Costs for Program/Project: $206

c. Cumulative Accrued Costs

Planned			0			80			135		206
Actual			0			19			54		100
Variance			0			61			81		106

11. Major Milestone Status	Units Planned / Units Complete	
6.3 Engineering Performance of Advanced Materials	P	
	C	■
6.5 Materials for Gas Separation	P	
	C	■
6.6 SiAlON Coatings for Alkali-Resistant Silicon Nitride	P	
	C	■
	P	
	C	
	P	
	C	
	P	
	C	
	P	
	C	
	P	
	C	

12. Remarks
The remainder of Year 3 , Task 6.3 -$16,000 was transferred to Year 4, Task 6.3.

13. Signature of Recipient and Date: 2/3/97

14. Signature of DOE Reviewing Representative and Date

FORM EIA-459E
(10/80)

U.S. DEPARTMENT OF ENERGY
FEDERAL ASSISTANCE MANAGEMENT SUMMARY REPORT

FORM APPROVED
OMB NO. 1900 0127

1. Program/Project Identification No.	2. Program/Project Title	3. Reporting Period
DE-FC21-93MC30097	TASK 6.0 HIGH-TEMPERATURE MATERIALS	10-1-96 through 12-31-96

4. Name and Address
Energy & Environmental Research Center
University of North Dakota
PO Box 9018, Grand Forks, ND 58202-9018 (701) 777-5000

5. Program Start Date: 01-12-93

6. Completion Date: 12-31-97

Milestone ID. No.	Description	Planned Completion Date	Actual Completion Date	Comments
Subtask 6.3	Engineering Performance of Advanced Materials			All milestones should be moved back 3 months to reflect the late start of the work.
a	Complete joining tests of silicon carbide using Joule heating	9/96		
b	Complete joining tests of silicon nitride with SiAlON	9/96	9/96	*
c	Complete corrosion tests of ceramic joints	12/96		
d	Complete corrosion tests of high-temperature alloys	12/96		
Subtask 6.5	Materials for Gas Separation			
a	Complete preparation of substoichiometric aluminosilicate membranes with the electron-beam coater	9/96		
b	Complete testing of hydrogen and hydrogen disulfide permeability of the substoichiometric aluminosilicate membrane	12/96		
Subtask 6.6	SiAlON Coatings for Alkali Resistant Silicon Nitride			
a	Determine morphologic and mechanical properties of alkali vapor-corroded SiAlON	9/96	12/96	
b	Determine morphologic and mechanical properties of coal slag-corroded SiAlON	12/96	12/96	

* Moved to Subtask 6.6 for reporting

Report Number (14) DOE/MC/30097--5592

Publ. Date (11) 19970708

Sponsor Code (18) DOE/FE, XF

JC Category (19) UC-101, DOE/ER

DOE